Probing superlattices of silicon/silicon-germanium alloy with raman spectroscopy

Lockwood, David J.

Publisher's version / Version de l'éditeur:

Physics in Canada, 43, 2, pp. 70-74, 1987-03

Probing Superlattices of Silicon/Silicon-Germanium Alloy with Raman Spectroscopy

David J. Lockwood
Laboratory for Microstructural Sciences,
Division of Physics,
National Research Council,
Ottawa, Ontario K1A 0R6

Solid-state physics has branched out in a new direction now that the production of superlattices has become possible. A superlattice is a crystal made up of layers of different materials such that a new periodic structure is formed. These superlattices are commonly made by molecular beam epitaxy (MBE), wherein two or more molecular beams are directed at a substrate with the desired crystallographic orientation, while switching the beams in timed intervals to produce the periodicity and structure desired. To form the superlattices described in this article a silicon beam remains switched on, while the germanium beam is switched on and off to form the alloy layers.

1. Introduction

Raman scattering spectroscopy has been widely used to characterize the physical properties of semiconductors for at least 20 years.[1] In Raman scattering experiments, monochromatic laser light is focused on the sample and the light scattered inelastically by excitations in the solid is collected and spectrum analyzed. The frequency shifts of the peaks in the Raman spectrum from the laser line position give the energies of the fundamental excitations, which may be electronic or vibrational. More recently, the technique has proved especially valuable for evaluating the mechanical and electronic properties of strained layer superlattices.[2] In particular, for the $Si/Si_{1-x}Ge_x$ system, Raman scattering has been used to evaluate the strain within the alloy and Si layers.[3,4]

This article reviews our recent work on light scattering studies of the phonons in both $Si_{1-x}Ge_x$ strained layer superlattices and thick $Si_{1-x}Ge_x$ layers with germanium concentrations in the range $0.2 < x < 0.5$. The results obtained from a study of the longitudinal acoustic and optic phonons have provided information on the crystalline quality, on the strain within the superlattice layers and on a special kind of order within the alloy layers.

2. Material preparation and measurements

Several $Si/Si_{1-x}Ge_x$ superlattices of various Si thicknesses d_1, alloy thicknesses d_2 and composition x were deposited on (100) Si substrates in a Vacuum Generator V80 system.[5] The layers were grown by molecular beam epitaxy (MBE) at temperatures below 550°C. Several thick ($\sim 1\ \mu m$) single layers of $Si_{1-x}Ge_x$ were also grown this way, but at different temperatures in the range 500 to 800°C. The superlattices have been assessed by Rutherford back scattering, x-ray diffraction and cross-sectional transmission electron microscopy (TEM).[6] The epitaxial material was found to be of excellent crystalline quality, and the $Si/Si_{1-x}Ge_x$ interfaces were shown to be commensurate. In $Si/Si_{1-x}Ge_x$ superlattices grown on Si, the lattice mismatch is accommodated by a tetragonal distortion of the alloy layers. The tetragonal distortion was investigated using x-ray diffraction and the measured strain was in good agreement with classical elastic theory.

The Raman scattering measurements were carried out using the 90° scattering geometry depicted in Fig.1. This configuration resulted in low stray light intensities and allowed measurement of the Raman spectrum at frequency shifts less than 4 cm^{-1}. The spectra were excited with 300 mW of 457.9 nm argon laser light and with $\theta = 12.3°$, which corresponds to Brewster's angle at this wavelength. Under these conditions, and with laser light polarized along Y, the maximum Raman signal was obtained from the sample with respect to any substrate signal. This is because the sampling depth, where 90% of the incident light intensity has been absorbed, is only ~ 650 nm at 457.9 nm. Because of the high refractive index (n — 4.6 at 457.9 nm), the Brewster angle scattering configuration corresponds nearly to back scattering *within* the sample. The scattered light was analyzed with a Spex double monochromator, detected with a cooled RCA 31034A photomultiplier, and recorded under computer control. All measurements were carried out at room temperature in a helium gas atmosphere, which was used to eliminate air features from the spectrum.

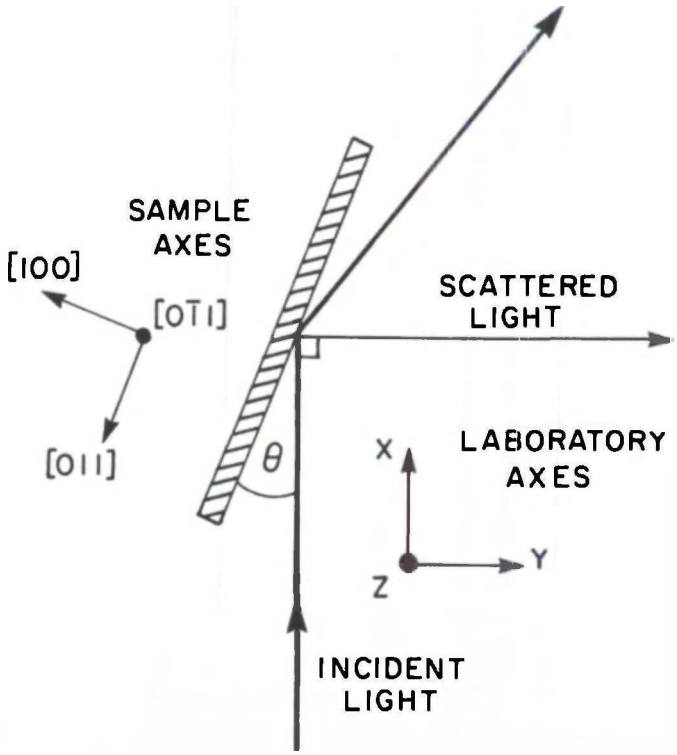

Fig. 1. A Raman scattering experiment. The specimen under examination is shown in section, shaded. Laser light is incident at the Brewster angle, 77.7 degrees for this sample. Light scattered at wavelengths near that of the incident light is analysed with a monochromator.

3. Acoustic phonons

Low frequency Raman spectra obtained from two superlattices are shown in Fig. 2. These results are typical of the other superlattices in that all gave a number of sharp lines in the low-frequency Raman spectrum, but the number of lines and their frequencies were strongly dependent on the layer thicknesses and, to a lesser extent, on the x value. These lines are all attributed to zone-folded longitudinal acoustic modes.

The existence of a reduced Brillouin zone in the superlattice substantially modifies the phonon spectrum through the "folding" of the original dispersion curves into the new minizone.[7] Small gaps are created at zero wave vector and at the minizone boundary given by $q_{MZ} = \pi/d$, where $d = d_1 + d_2$ is the superlattice periodicity. Denoting the minizone centre frequencies by $\omega = m\omega_0$, where m = 0,1,2,. . . . is the folding index, light scattering peaks should occur at $\omega = m\omega_0 \pm q_P V_{SL}$. Here q_P is the momentum transferred in the scattering event and V_{SL} is the superlattice sound velocity. Thus for each folding index $m \neq 0$ there exists a doublet m− and m+ corresponding to $-q_P V_{SL}$ and $+q_P V_{SL}$, respectively; the case m = 0 corresponds to the usual Brillouin scattering from the acoustic mode. As an example, we have labelled some of the peaks in Fig. 2(b) in this notation. Since the observed frequency shifts are small, Rytov's theory of acoustic vibrations in layered media[8] may be applied; it predicts $\omega_0 = V_{SL}(2\pi/d)$ assuming linear dispersion. The observed peak frequencies and intensities agree very well with theory following the Rytov model[9], as can be seen in Table 1. The calculations required values for d_1, d_2 and x that agreed within error to values determined by other techniques. Hence the light scattering from folded acoustic modes may be used to accurately determine average values for d_1, d_2 and x. At present, information on the variation of d_1, d_2 and within the superlattice must be obtained using other techniques, although an analysis of the phonon linewidths would also be useful in this respect.

The intensity of the folded acoustic modes is related to interface quality[10] and annealing the superlattices at 850°C for 30 minutes completely removes these lines from the spectrum, as can be seen for example in Fig. 4 (b). The interface sharpness determines not only the overall intensity but also the number of lines (i.e., the maximum value of $m = m_{max}$) observed. The quantity of interest is d/m_{max}, which for our

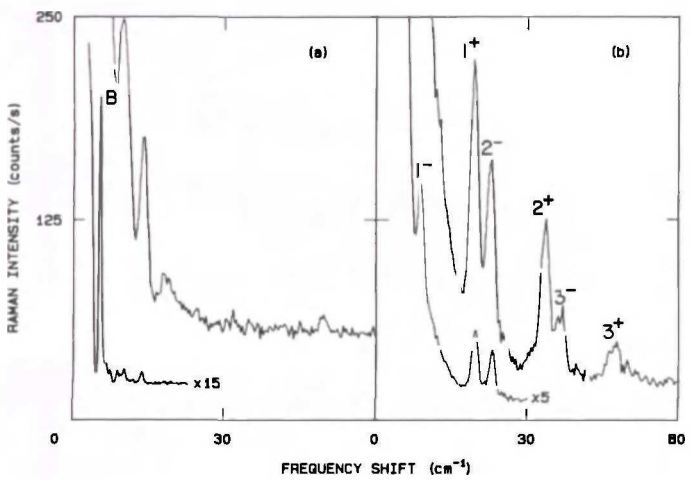

Fig. 2. The low-frequency Raman spectrum of (a) the 10th generation Fibonacci superlattice (MBE-106) shown in Fig. 3 constructed from blocks of Si 20 nm thick and $Si_{0.88}Ge_{0.12}$ 9 nm thick, and (b) commensurate strained-layer superlattice (MBE-35) comprising 40 periods of Si/$Si_{0.7}Ge_{0.3}$ with d_1 =14.5 nm and d_2 = 4.0 nm. Note that the Brillouin peak (B) is clearly resolved in these Raman experiments due to the high optical quality of the sample. The spectral resolution is 1.6 cm^{-1} for both upper traces, and 0.5 and 1.1 cm^{-1} for the reduced-sensitivity lower trace in boxes (a) and (b), respectively.

Table 1. Experimental and calculated peak frequencies and intensities of lines in the Raman spectrum of sample MBE-35, taking d_1 = 14.9 nm, d_2 = 4.3 nm and x = 0.3. The calculated intensity is normalized to agree with the mean experimental intensity for folding index m = 1.

Index m	ωexpt (cm^{-1})	ωcalc (cm^{-1})	I_{expt} (counts/s)	I_{calc}
0	5.4	5.4	2000	—
1−	9.0	8.8	260	200
1+	20.0	19.5	170	200
2−	23.3	22.9	120	120
2+	34.3	33.7	96	120
3−	37.1	37.1	40	40
3+	47.6	47.9	22	40
4−	50.9	51.2	9	4
4+	60.8	62.0	5	4
5−	64.3	65.4	2	3
5+	—	76.2	—	3

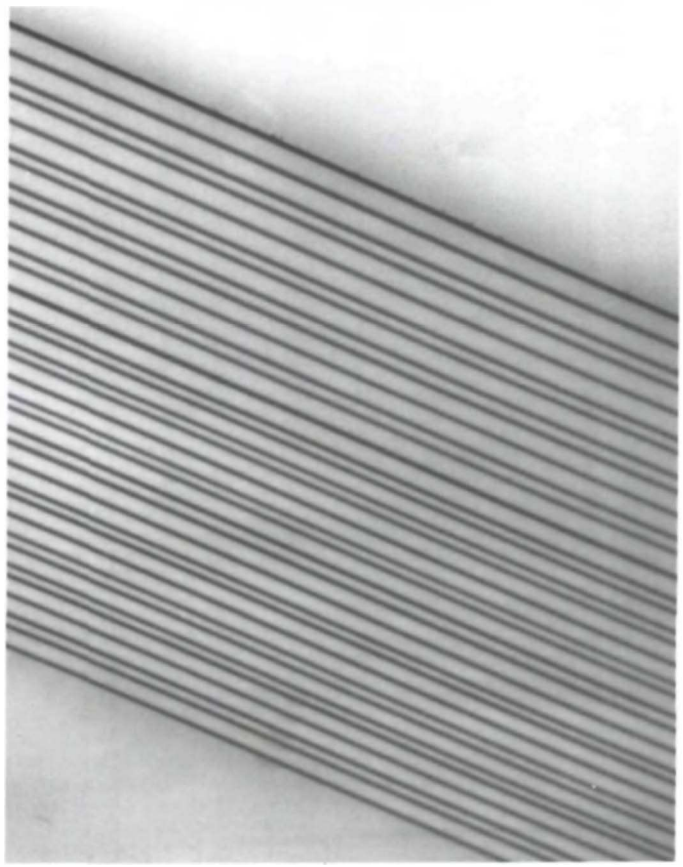

Fig. 3. A transmission electron micrograph of the 10th generation Fibonacci superlattice MBE-106 in a [110] cross section. The dark layers correspond to the silicon-germanium alloy, and the substrate is at the bottom of the figure. (Micrograph kindly provided by J.-M. Baribeau, NRC).

annealed samples is ~ 4 nm. This implies a disturbance in the *electron* density profile at the interface of about 4 nm at most. We know from TEM measurements that the *atomic* interfaces are sharper than this (≤ 1 nm). The annealed superlattices show no difference in the interfacial abruptness when observed by high resolution TEM[11], since the Si diffusion length is only of the order of the unit cell dimension (~ 0.5 nm).[12] Thus, despite the fact that the Raman scattering is mediated by the electrons, the intensities of the folded modes are very sensitive to interfacial quality at the atomic scale. Further work on relating the overall Raman intensity to the interface quality is in progress.

4. Optic phonons

The Raman spectrum at higher frequencies exhibits first-order features characteristic of the silicon and alloy layers, and sometimes (for thinner samples) a line at 520 cm $^{-1}$, which corresponds to scattering from the longitudinal optical phonon in the underlying Si buffer layer and substrate. Many specimens comprising both superlattices and single thick layers were studied and a representative Raman spectrum is shown in Fig. 4 (a). The strained-layer superlattice spectrum of Fig. 4 (a) shows strong phonon peaks at 294.5, 414.9, 505.9 and 517.3 cm $^{-1}$ that are attributed to scattering from longitudinal optic phonons in either the alloy (labelled Ge-Ge, Ge-Si and Si-Si in the notation of Ref. 13) or silicon (Si) layers, respectively. A layer spectrum of $Si_{0.8}Ge_{0.2}$, for example, show similar Ge-Ge, Ge-Si and Si-Si peaks at 286.0, 404.4 and 507.8 cm $^{-1}$, respectively. The thick layer is in a relaxed state in this sample.

The Si line for most of the superlattices grown on a Si buffer layer occurs at a frequency that is close to the bulk Si value of 520 cm^{-1}, indicating there is little strain in the Si layers.

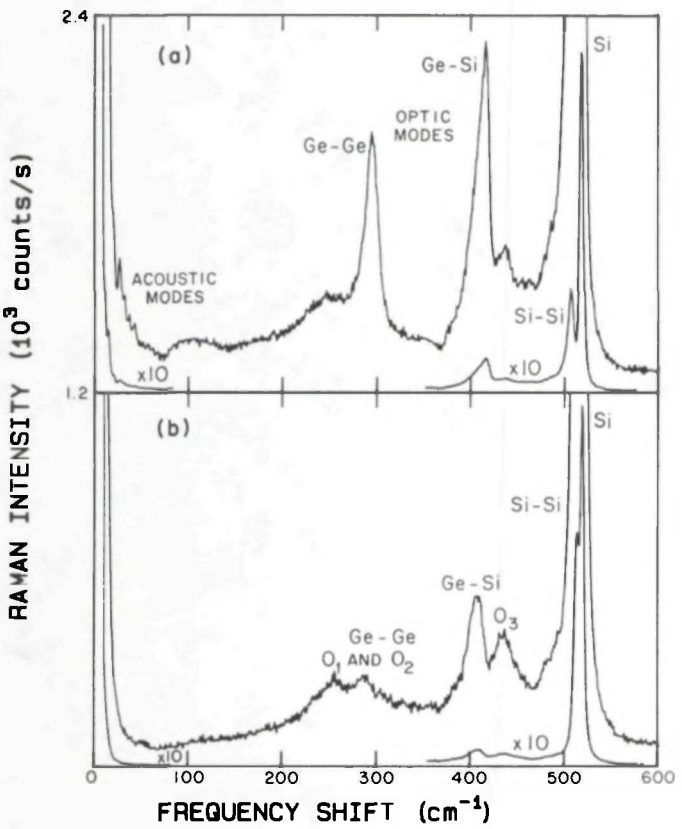

Fig. 4. The Raman spectrum of strained-layer superlattice MBE-26 comprising 21 periods of Si 45 nm thick and $Si_{0.67}Ge_{0.33}$ 20 nm thick: (a) as grown and (b) after annealing for 30 min. at 850°C.

However, in a sample (MBE-111) grown on a buffer layer of $Si_{0.8}Ge_{0.2}$, the Si line was at 513.8 cm $^{-1}$. This shift $\Delta\omega$ of approximately 6 cm $^{-1}$ to lower frequency indicates that there is a large biaxial stress in the Si layers. From the experimentally determined relationship [4,14] $\sigma = (2.49\ \text{kbar/cm}^{-1})\Delta\omega$ between the stress σ and $\Delta\omega$ we find a stress of 15 kbar in the Si layers of this superlattice.

The alloy line positions in the Raman spectra of several thick relaxed epilayers, as-grown superlattices and partially relaxed superlattices are summarised in Fig. 5. The solid curves are the experimental data of Brya[13] obtained from bulk *polycrystalline* $Si_{1-x}Ge_x$, and there is good agreement with the present results obtained from *single-crystal* layer specimens. The three alloy lines in the strained-layer superlattices are higher in frequency by as much as 10 cm $^{-1}$ for higher x values, indicating a considerable lateral compressive strain in the alloy layers. As there has been no axial pressure dependent study of $Si_{1-x}Ge_x$, as was done for Si,[14] the Raman results cannot be used in this case to determine the stress directly in kbar units. However, the Raman peaks shift linearly with layer strain[1] and can be correlated with other direct measures of alloy strain such as the tetragonal distortion.

Annealing the superlattices at 850° for 30 min. results in the alloy lines generally shifting down in frequency toward the equivalent relaxed-alloy line positions (see Figs. 4 and 5) consistent with a partial relaxation of misfit strain. This fact together with the small characteristic diffusion length (~ 0.5 nm at 850°C) in the annealing suggests that plastic relaxation and not interdiffusion is the main source of the changes in the optic-mode spectral features.[11]

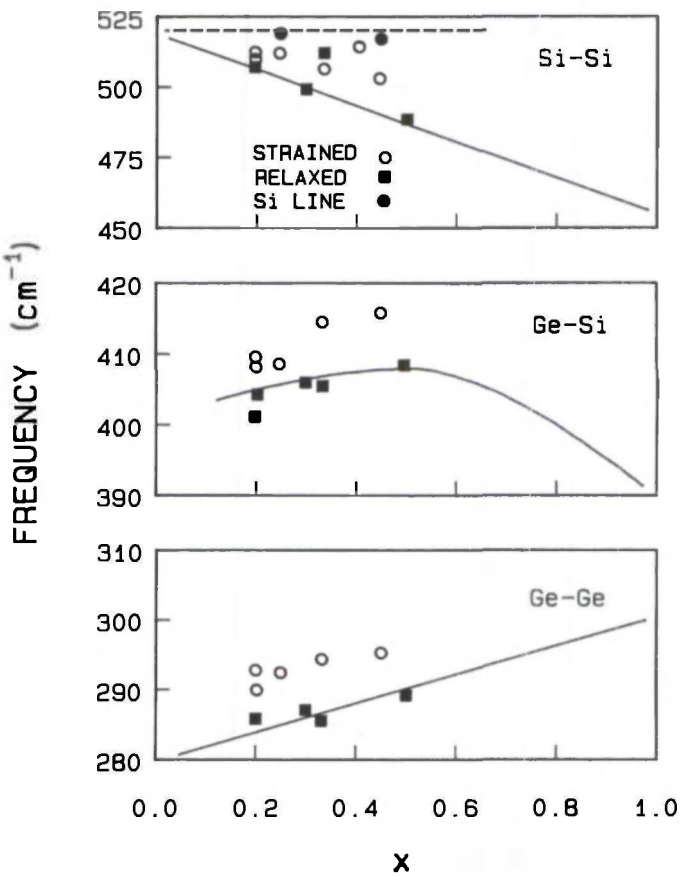

Fig. 5. The concentration dependences of the frequencies of the three first-order Raman lines of $Si_{1-x}Ge_x$ in superlattices and thick epilayers compared with measurements[13] of unstrained polycrystalline material (full lines). The broken line represents the Si line frequency in unstrained silicon.

Figs. 4 (a) and (b) also exhibit a weak line near 435 cm^{-1} (0_3) and another weaker line is visible near 225 cm^{-1} (0_1). Both of these extra peaks are seen to varying extent in most specimens, with the ~ 435 cm^{-1} line sometimes as strong as the ~ 410 cm^{-1} Ge-Si alloy line. The lines are too sharp and their intensities are too high for them to be attributed to second order scattering. Their frequencies shift by up to 10 cm^{-1} with type of specimen, strain and Ge concentration. An increase or decrease in intensity of these lines from sample to sample correlates with an increase or decrease of the intensity of the dark-field TEM image of an extra ½ (111) reflection plane.[15] Ourmazd and Bean[16] have shown that a Laue diffraction pattern exhibiting such extra reflections can arise from a new primitive unit cell with twice the original lattice period in a <111> direction. They attribute the presence of such ½ (111) reflections to long range ordering of Si and Ge atoms in the alloy.

The longitudinal optic mode frequencies for the Ourmazd and Bean unit cell have been calculated in a model based on effective nearest-neighbor force constants for central forces between rigid atoms.[15] The Ge-Ge, Ge-Si and Si-Si effective force constants were determined from the appropriate reduced masses and the frequencies of the respective alloy lines in the *same* Raman spectrum. The three calculated frequencies resulting from this model lie near 250, 295 and 440 cm^{-1}. The first (0_1) and the last (0_3) of these correspond closely to the extra peaks near 255 and 435 cm^{-1}, while the second one (0_2) at the 295 cm^{-1} would underlie the stronger Ge-Ge peak at ~ 290 cm^{-1} and is thus not visible directly in the experiment (see Fig. 4 (b)). The frequency shift from sample to sample of the ~ 435 cm^{-1} line corresponds to within 1 cm^{-1} with the corresponding shift of the calculated frequency of the 0_3 line. This good agreement between the calculated and experimental frequency shifts indicates that the Ourmazd and Bean ordering is responsible for the extra Raman lines near 255 and 435 cm^{-1}.

The epitaxial growth of GaAs on Si is of current interest because it would allow the high-speed and optical properties of GaAs to be combined with the well-developed Si technology. As the first step in obtaining good quality epitaxial material of this type, the MBE Section in the Laboratory for Microstructural Sciences has been growing single crystal Ge on Si.[17] The Ge is being used as a buffer layer in this case, since the lattice parameters and thermal expansion coefficients of Ge and GaAs are a much closer match than those of Si and GaAs. Raman scattering studies of these Ge films have provided confirmation of their single crystal nature. A slight (less than 1 cm^{-1}) upward or downward shift in the position of the longitudinal optical phonon (at 300 cm^{-1} in unstrained Ge) correlates well with the small compressive or extensive strain found in the Ge layer at room temperature. This residual strain arises from the contraction of the crystal on cooling after layer growth and its extent is dependent on the growth temperature.[17] Raman scattering can be used in principle to characterize the residual strain.

5. Fibonacci superlattices

The Fibonacci sequence, which is defined by the elementary recursion $f_{n+2} = f_n + f_{n+1}$ with $f_0 = 0$ and $f_1 = 1$, has a long history. It was derived by the mathematician Leonardo of Pisa or Leonardo Fibonacci (12th-13th Century) from consideration of a problem posed in his book "Liber abaci" published in 1202:

> "A certain man put a pair of rabbits in a place surrounded on all sides by a wall. How many pairs of rabbits can be produced from that pair in a year if it is supposed that every month each pair begets a new pair which from the second month on becomes productive?"

The properties of the Fibonacci numbers have been extensively studied, resulting in a considerable literature. For example, Robert Simson at Glasgow University noted in 1753 that as the numbers increased in magnitude, the ratio between succeeding numbers approached the golden number, section or mean $\tau = (1+\sqrt{5})/2 \sim 1.618$. The inverse of τ is $\tau^{-1} = (\sqrt{5}-1)/2 - 0.618$ and both are roots of $\tau^{-2}-\tau^{-1} = 0$, an equation derived from the Divine proportion of the 15th-Century Italian mathematician Lucas Pacioli.

The genesis of a Fibonacci superlattice can be followed using the rule that the n-th generation of the structure is formed by combining the (n-2) generation structure with the (n-1) generation structure. Thus, if the first generation structure is A, and the second generation structure is BA, then the third generation structure will be ABA, the fourth BAABA, etc. The example in the text can be subdivided as follows:

1	2	3	4	5	6
A	BA	ABA	BAABA	ABABAABA	BAA. . . .etc.

The 10th generation Fibonacci superlattice referred to in Fig. 2 is formed by depositing the epitaxial layers according to the 10th generation structure.

Fibonacci sequences have recently become very interesting in solid state physics, because they are one-dimensional analogues of the Penrose lattice in two dimensions and the icosohedral group in three dimensions. Developments in the theory of a Fibonacci type of quasiperiodic structure were recently tested with the first realization of an actual crystal based on an incommensurate superlattice.[18] The crystal, grown by MBE, consisted of alternating layers of GaAs and AlAs to form a Fibonacci sequence.

We have studied the Raman spectrum of similar quasiperiodic superlattices constructed according to the Fibonacci sequence from two basic building blocks A and B of Si (thickness d_A) and $Si_{1-x}Ge_x$ (thickness d_B), respectively. The superlattice structure in terms of these building blocks looks like

ABAABABAABAABABAABABA etc.

The effective lattice parameter of such superlattices is $\bar{d} = d_A \tau + d_B$. Although the Raman spectrum of the optic modes looks much the same in commensurate and incommensurate superlattices grown using the same building blocks, the folded acoustic mode spectrum looks very different. As can be seen from a comparison of Figs. 2 (a) and 2 (b), the peak frequencies in the Fibonacci superlattice do not follow the normal periodic sequence of the commensurate superlattice and the intensities of the peaks do not follow the usual order either.

The acoustic phonon spectrum can be analyzed in much the same way as the commensurate case with due allowance for the quasiperiodicity.[19] The quasiperiodic minizone boundary is now given by $q_{MZ} = \pi/\bar{d}$ and the Raman peaks occur at $\omega = \omega_0(m+n\tau) \pm q_P V_{SL}$. There are now two indices m and n to contend with, but it turns out that the most intense lines occur when m and n are both small Fibonacci numbers. In this case $m+n\tau=\tau^P$ and so only one integer index p is needed to describe the spectrum. The Raman spectrum of another Fibonacci superlattice is shown in Fig. 6, where assignments are made in terms of the index p (the + and – signs refer, as before, to the $\pm q_P V_{SL}$ term). Calculations of the acoustic mode frequencies are in excellent agreement with experiment, as can be seen from Table 2. These experiments have provided the first definitive test of models for the lattice dynamics of a Fibonacci lattice.

Table 2. Experimental and calculated peak frequencies for prominent lines in the Raman spectrum of sample MBE-124G. The peaks expected at low frequency are masked by the Brillouin peak (B) in the experiment.

Index			ωexp	ωcalc
m	n	p	(cm^{-1})	(cm^{-1})
2^-	-1	-2^-	—	2.6
0	0	B	5.3	5.2
-1^-	1	-1^-	—	7.8
2^+	-1	-2^+	13.5	13.4
1^-	0	0^-	15.7	15.8
-1^+	1	-1^+	18.5	18.1
1^+	0	0^+	26.9	26.1
0^-	1	1^-	29.2	28.7
0^+	1	1^+	39.9	38.9
1^-	1	2^-	51.0	49.7
1^+	1	2^+	60.9	59.9

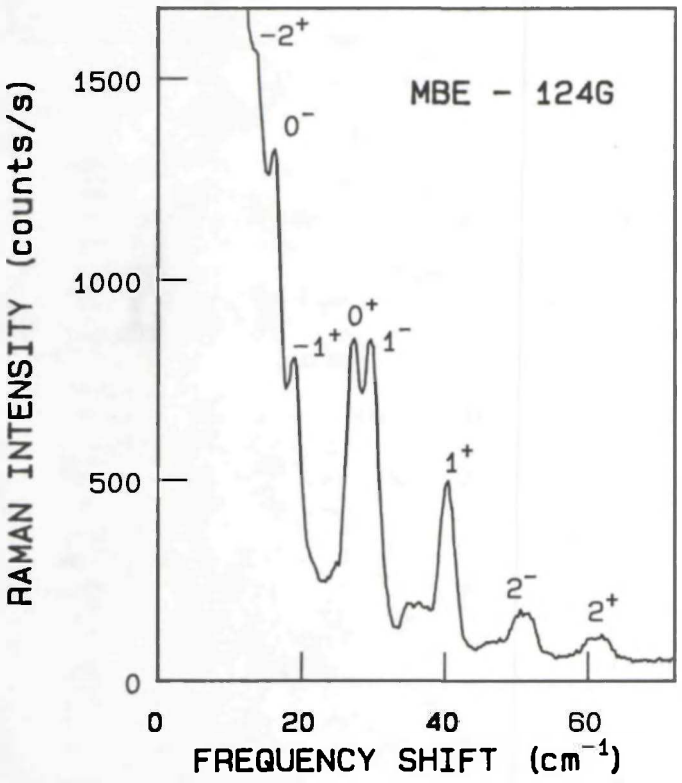

Fig. 6. The Raman spectrum of the 11th-generation Fibonacci superlattice MBE-124G constructed from blocks of Si 5.4 nm thick and $Si_{0.52}Ge_{0.48}$ 4.2 nm thick.

6. Conclusions

This review of Raman scattering from MBE grown $Si/Si_{1-x}Ge_x$ superlattices and $Si_{1-x}Ge_y$ layers has shown that considerable physical information can be derived from the phonon spectrum. The acoustic phonon scattering in superlattices can be used to obtain precise average layer thicknesses and x values, and it can give qualitative information on the interface quality. In this last respect Raman scattering is better than many other direct measurement techniques. The optic phonons can provide quantitative information on the strain within layers, on the overall quality of the layers (from the phonon linewidths[3]), and on the existence of weak long-range ordering of Si and Ge atoms, which is found to occur to varying extent in all of the alloy layers we have studied. Finally, Raman scattering possesses the distinct advantage of being a non-destructive probe of crystalline perfection.

Acknowledgement

The excellent crystals used in the work reported here were grown at NRC by J.-M. Baribeau, M.W. Denhoff and D.C. Houghton, and various aspects of the theoretical work are due to M.W.C. Dharma-wardana, E.W. Fenton, and A.H. MacDonald.

References

1. See, for example, W. Hayes and R. Loudon, "Scattering of Light by Crystals" (Wiley, New York, 1978).
2. See, for example, J.C. Bean, Mat. Res. Soc. Symp. Proc. **37**, 245 (1985), and F. Cerdeira, A. Pinczuk, T.H. Chiu and W.T. Tsang, Phys. Rev. **B32**, 1390 (1985).
3. F. Cerdeira, A. Pinczuk, J.C. Bean, B. Batlogg and B.A. Wilson, Appl. Phys. Lett. **45**, 1138 (1984).
4. G. Abstreiter, H. Brugger, T. Wolfe, H. Jorke and H.J. Herzog, Phys. Rev. Lett. **54**, 2441 (1985).
5. This system and the MBE crystal growing technique has been described in an earlier article by Chandre Dharma-wardana, Physics in Canada **42** (No. 4), 81 (1986).
6. J.-M. Baribeau, D.C. Houghton, D.J. Lockwood and T.E. Jackman "Semiconductor-Based Hetero-Structures; Interfacial Structure and Stability", M.L. Green et al. Eds. (Metallurgical Society, Warrendale, 1986) p. 185.
7. The zone folding of acoustic modes is well described in Ref. 5.
8. S.M. Rytov, Akust. Zh. **2**, 71 (1956) [Sov. Phys.-Acoust. **2**, 68 (1956)].
9. M.W.C. Dharma-wardana, D.J. Lockwood, J.-M. Baribeau and D.C. Houghton, Phys. Rev. **B34**, 3034 (1986) and Phys. Rev. **B35**, in press.
10. C. Colvard, T.A. Grant, M.V. Klein, R. Merlin, R. Fischer, H. Morkoc and A.C. Gossard, Phys. Rev. **B31**, 2080 (1985).
11. D.C. Houghton, D.J. Lockwood, M.W.C. Dharma-wardana, E.W. Fenton, J.-M. Baribeau and M.W. Denhoff, J. Crystal Growth (to be published).
12. S.M. Sze, "Physics of Semiconductor Devices" (Wiley, New York, 1981) p. 68.
13. See W.J. Brya, Solid State Commun. **12**, 253 (1973) and references therein for the origin of this notation.
14. M. Chandrasekhar, J.B. Renucci and M. Cardona, Phys. Rev. **B17**, 1623 (1978).
15. D.J. Lockwood, K. Rajan, E.W. Fenton, J.-M. Baribeau and M.W. Denhoff, Solid State Commun. (to be published).
16. A. Ourmazd and J.C. Bean, Phys. Rev. Lett. **55**, 765 (1985).
17. J.-M. Baribeau, T.E. Jackman, P. Maigné, D.C. Houghton and M.W. Denhoff (to be published).
18. R. Merlin, K. Bajema, R. Clarke, F.-Y. Juang and P.K. Bhattacharya, Phys. Rev. Lett. **55**, 1768 (1985).
19. G.C. Aers, D.J. Lockwood, M.W.C. Dharma-wardana, A.H. MacDonald, J.-M. Baribeau and D.C. Houghton, American Physical Society March Meeting, New York (1987).